Korean J. Chem. Eng., 35(8), 1642-1649 (2018)
DOI: 10.1007/s11814-018-0078-9

pISSN: 0256-1115
eISSN: 1975-7220

Adsorption of carbon dioxide and water vapor on fly-ash based ETS-10

Yushun Wang*, Tao Du*,†, Xin Fang*,, Da Meng*, Gang Li**,***, and Liying Liu*,***,†**

*State Environmental Protection Key Laboratory of Eco-Industry, Northeastern University, Shenyang, China
**Department of Chemical and Biomolecular Engineering, The University of Melbourne, Melbourne, Australia
***ARC Centre for LNG Futures, The University of Western Australia, Crawley, Australia
(*Received 9 January 2018 • accepted 10 May 2018*)

Abstract−CO_2 capture from humid flue gas is always costly due to the irreplaceable pretreatment of dehydration in current processes, which creates an urgent demand for moisture-insensitive adsorbents with considerable CO_2 uptakes as well as remarkable H_2O tolerances. In the present work, the microporous titanium silicate molecular sieve ETS-10 was synthesized with coal fly ash as the only silica source. The as-synthesized ETS-10 was characterized by X-ray diffraction, scanning electronic microscopy and infrared spectroscopy to verify its crystal morphology, in which neither impurity nor aggregation was observed. The following CO_2 adsorption experiments on the thermal gravimetric analyzer demonstrated its similar CO_2 adsorption capacity yet dramatical adsorption kinetics among some other microporous materials, e.g., potassium chabazite. These specific properties consequently guaranteed its favorable CO_2 adsorption capacity even at high temperatures (1.35 mmol/g at 393 K) and shortened the breakthrough time of single CO_2 flow to less than 20 s. In CO_2/H_2O binary breakthrough experiments, the as-obtained ETS-10 still maintained excellent CO_2 uptake of 0.81 mmol/g at 323 K, regardless of the presence of water vapor, making it a promising substitute for direct CO_2 separation from humid flue gases at practical conditions of post-combustion adsorption.

Keywords: ETS-10, Fly Ash, CO_2, Binary Adsorption, Humid Flue Gas

INTRODUCTION

Humans are suffering from the impacts of climate change, e.g., glacier melting, oceans expanding, unpredictable extreme climate events, threatening our developments as never before. Scientists have concluded that climate change could be mainly attributed to the increasing CO_2 emission. Therefore, carbon dioxide emission reduction has attracted worldwide attention [1].

There are many strategies for CO_2 capture under investigation, including pressure swing adsorption (PSA) [2,3], temperature swing adsorption (TSA) [4], chemical absorption [5], cryogenic [6] and membrane separation [7]. PSA is especially promising due to its low energy consumption, high economic efficiency, wide application, etc. [8,9]. However, this is not the case in humid flue gas separation. Most common adsorbents such as activated carbon, zeolites [10-12], metal-organic frameworks (MOFs) [13-15] and zeolitic imidazolate frameworks (ZIF) [16,17] will promptly deactivate in the presence of water vapor because H_2O molecules bind much tighter with the adsorbent than CO_2 molecules and are thus hard to remove. Consequently, adsorption sites are prior occupied by the former, leading to striking decreases of CO_2 adsorption capacities. Currently, dehydration of humid flue gas is usually inevitable to ease defects of water, greatly elevating the costs. Meanwhile, the manufacture of adsorbents has already constituted approximately 70% of the total cost of practical PSA process, so that an efficient adsorbent with lowered preparation cost and improved water tolerance is expected to effectively expand the applications of PSA by eliminating dehydration pretreatments.

ETS-10 is a type of microporous titanium silicalite molecular sieve first reported by Kuznicki et al. in 1989 with an ideal molecular formula of $(Na, K)_2TiSi_5O_{13}{\cdot}4H_2O$ [18]. This microporous titanosilicate with an effective pore size of approximately 8 Å exhibits favored thermal stability, prominent cation exchange capacity and considerable adsorption properties. ETS-10 has been widely used in acid-base catalysis, photocatalysis, gas separations [19-21]. In 2015, Shuavo [22] reported that framework structures of ETS-10 could keep stable even in a hot and humid environment. We suppose this property will endure ETS-10 favorable CO_2 adsorption performance in the practical exhaust gases of post-combustion, which is usually ~65-120 °C, containing ~10 wt% H_2O. However, CO_2 adsorption performance of ETS-10 in the humid environment, especially synthesis with cheap raw material of coal fly ash and anatase, has not been studied yet.

In this study, ETS-10 was synthesized with coal fly ash. We further characterized the sample with X-ray diffraction (XRD), Fourier-transform infrared spectroscopy (FTIR), scanning electron microscopy (SEM) to observe its microstructures. Finally, the potential of CO_2 capture from humid flue gases by using our as-synthesized product was investigated.

MATERIALS AND METHODS

1. Preparation of ETS-10 with Coal Fly Ash

The silicium containing solution was first prepared by boiling the

†To whom correspondence should be addressed.
E-mail: dut@smm.neu.edu.cn, liuly@smm.neu.edu.cn

mixture of 60 g of coal fly ash (collected in a power plant in Inner Mongolia, China, SiO_2 48.5 wt%), 50 g of NaOH (SINOPHARM, 96.0%) and 150 g of deionized water under vigorous stirring (800 rpm) at 120 °C for 3 h. After filtration, hydrochloric acid (HCl, 35.0%) was added into the resulting supernatant dropwise to adjust the pH value to 11.2. Then, 3.6 g of Anatase (Aladdin, 99.8%) and 13.3 g of KCl (SINOPHARM, 99.5%) was added into the suspension, followed by vigorous stirring for 3 h at room temperature. The resulting suspension was transferred into a 250 ml Teflon-lined autoclave and heated at 230 °C for 24 h under a static condition. After cooling to ambient temperature, the resultant solid was collected by centrifugation, which was then washed three times with deionized water and dried at 110 °C for 5 h.

2. Characterization Methods

The structural property of prepared ETS-10 was analyzed by X-ray diffractometer (XRD-7000, Shimadzu) with a Cu Kα radiation source, and the tube voltage and tube current were 40 kV and 25 mA, respectively. Scanning electron microscopy (SEM) analysis was conducted using a field-emission scanning electron microscope (Superscan SSX-500, Shimadzu). Infrared spectroscopy was performed by Fourier transform infrared spectroscopy (Cary 660 FTIR, Agilent). N_2 adsorption-desorption isotherms were applied on the physisorption apparatus (JW-BK112, JWGB Sci&Tech.) at 77 K.

3. Adsorption Properties

3-1. Single Component Adsorption of CO_2

The adsorption isotherms of CO_2 on ETS-10 at different temperatures within 30-120 °C within a pressure range of 0-120 kPa were obtained on a physisorption apparatus (JW-BK112, JWGB Sci&Tech). CO_2 adsorption experiments of samples at 60 °C were also characterized by using the thermal gravimetric analyzer (STA 409PC, Netzsch). To further describe the CO_2 adsorption process on the prepared ETS-10, pseudo-first order kinetics model [23] and pseudo-second order kinetics model [24] were used in the data analysis.

3-2. Breakthrough Experiments

A custom-built adsorption apparatus (shown in Fig. 1) was used in single breakthrough experiments of H_2O and binary breakthrough experiments of CO_2/H_2O. This apparatus includes a humidity transmitter and an adsorption column. When the experiment is conducted, Ar and CO_2 are pre-mixed in a certain ratio by two mass flow meters. The mixed gas is then divided into two paths, where one path (humid gas) flows through a water bottle to carry the water vapor and the other one (dry gas) is connected to the column directly. The relative humidity of the gas was controlled by adjusting the flow ratios of dry and humid gases. The mixed gas was injected into the adsorption column, and the outlet humidity was measured by a humidity transmitter (Vaisala HUMICAP HMT 330, Finland).

In the CO_2/H_2O binary breakthrough experiment, the adsorption capacities of CO_2 and H_2O can be obtained by using a volumetric method. The calculation process is as follows.

The mass changes of the ETS-10 sample and water bottle were Δm_{sample} (g) and Δm_{bottle} (g), respectively. Then, the mass change of the prepared ETS-10 sample was calculated as

$$\Delta m_{sample} = m_{sample,\,i} - m_{sample,\,initial} \tag{1}$$

Water bottle weight change was calculated as

$$\Delta m_{bottle} = m_{bottle,\,initial} - m_{bottle,\,i} \tag{2}$$

The partial pressure of water vapor in air flow is P_{water}, which can be calculated by:

$$P_{water} = \frac{RH \times P_{sat,\,T}}{100} \tag{3}$$

where RH is the relative humility (%), $P_{sat,\,T}$ is the saturated vapor pressure at the adsorption temperature (kPa).

By measuring the contrast, the difference between atmospheric pressure and the air pressure in humidity transmitter is minor. For simplifying the calculation, the air pressure in the humidity transmitter was considered consistent with the atmospheric pressure. Then, the partial pressure of the carrier gas ($P_{carrier}$, kPa) is given by the following formula

$$P_{carrier} = P_{transmitter} - P_{water} \tag{4}$$

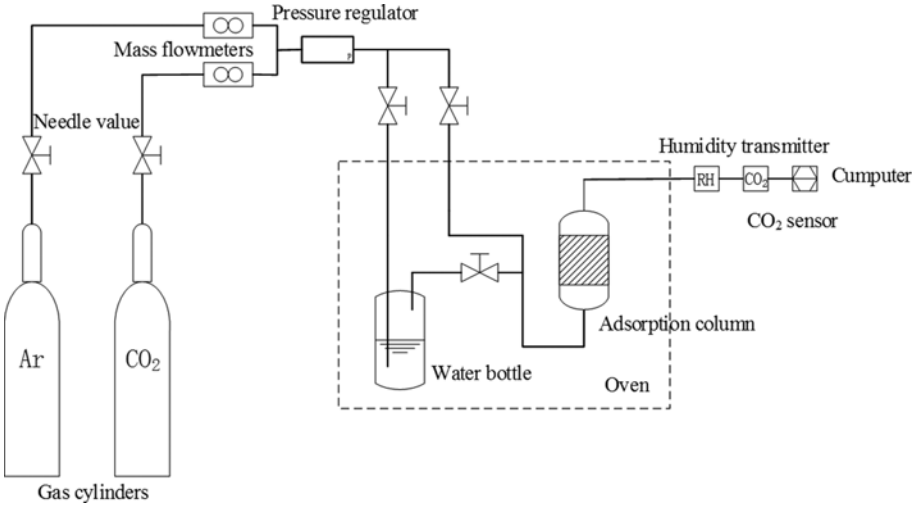

Fig. 1. Schematic diagram of the custom-built adsorption apparatus.

Mass flow in the humidity transmitter $q_{transmitter}$ (g/min) was the mass flow of the carrier gas plus the mass flow of water vapor. The formula is

$$q_{transmitter}=q_{carrier}+q_{water} \quad (5)$$

The volume flow was converted to the moles number by using the Dalton's law of partial pressure. Thus, the molar flow of carrier gas can be calculated by

$$q_{carrier(mol/min)}=\frac{q_{carrier}}{V_m\times 1000} \quad (6)$$

Herein, V_m represents the molar volume of gas at the experimental temperature (mL/mol).

Because $q_{water}\propto P_{transmitter}$, the molar flow of water vapor in the humidity transmitter can be calculated by

$$q_{water}=\frac{P_{water}\times q_{carrier}}{P_{carrier}} \quad (7)$$

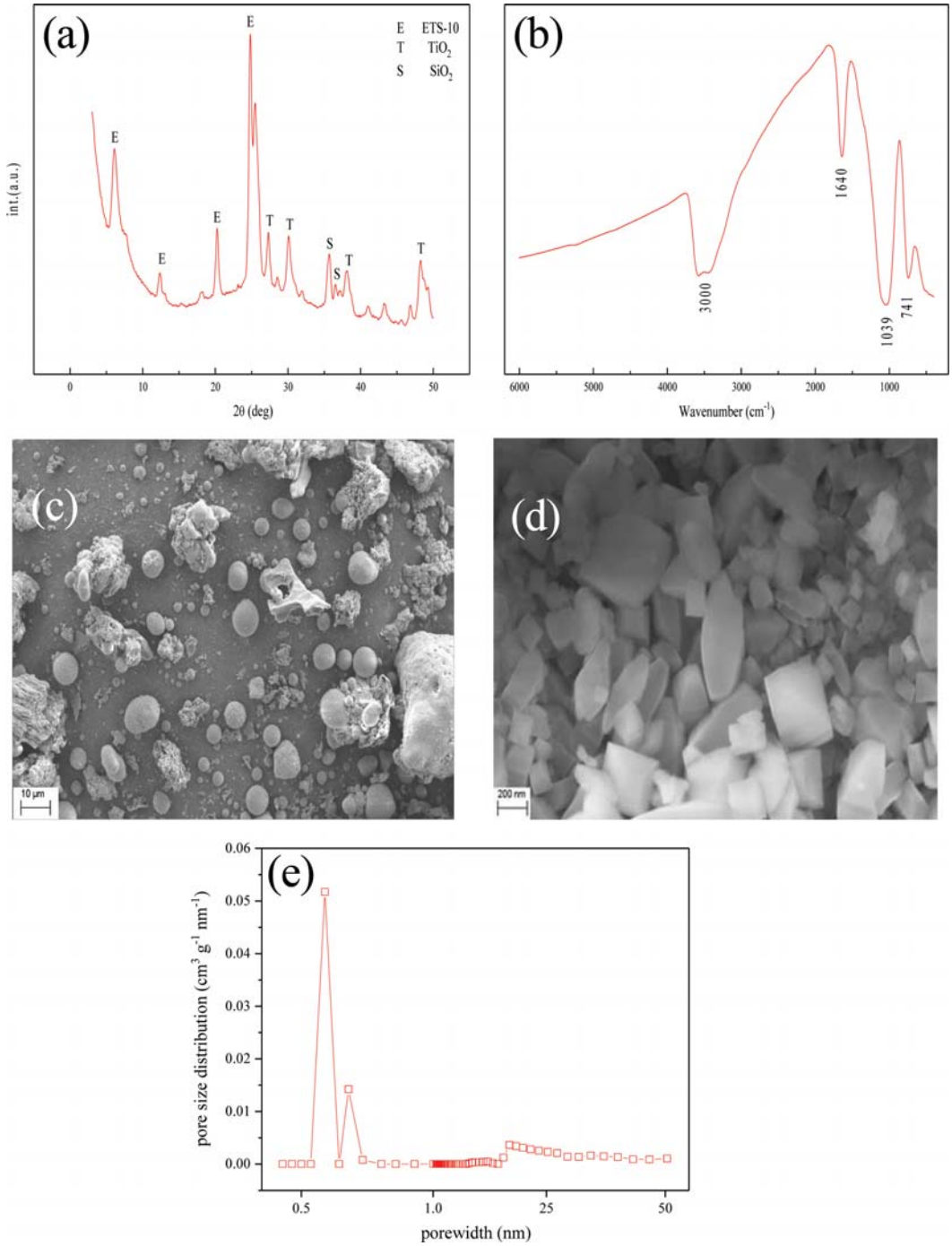

Fig. 2. Characterization of the ETS-10 sample: (a) XRD pattern, (b) IR spectra SEM (c) image of coal fly ash (d) and ETS-10 sample, (e) pore size distribution of ETS-10 sample.

The mass of water vapor passing through the humidity transmitter can be calculated from the following equation

$$n_{water,\,detected}=\sum_{i=1}^{n} q_{water,\,i}\Delta t \tag{8}$$

where Δt is the count time interval of humidity transmitter (s).

The mass of water vapor adsorbed on the synthesized ETS-10 sample was calculated by

$$m_{water}=\Delta m_{bottle}\times\left(1-\frac{n_{water,\,detected}}{n_{water,\,total}}\right) \tag{9}$$

Here Δm_{bottle} is the mass change of the water bottle (g), while $n_{water,\,total}$ represents the total mass of water vapor that can be detected in the absence of adsorbent (g). The adsorption amounts of CO_2 on the ETS-10 sample can be calculated by the following formula:

$$n_{CO_2}=\frac{q_{CO_2}\times t}{44}\times\left(1-\frac{\sum_{i=1}^{n}\varphi_{CO_2,\,i}}{n\times\varphi_{CO_2,\,n}}\right) \tag{10}$$

where $\varphi_{CO_2,i}$ represents the volume fraction of CO_2 in the exhaust gas (mL), i represents the reading sequence of CO_2 sensor. $\varphi_{CO_2,n}$ is the volume fraction of CO_2 when reaching the equilibrium (mL), while q_{CO_2} is the mass of CO_2 that flows through the mass flow meter per minute (g/min).

RESULTS AND DISCUSSION

1. Characterizations of Fly-ash Based ETS-10

The XRD pattern and IR spectra of the prepared ETS-10 are shown in Fig. 2. The product has distinct peaks at 2θ=6, 12, 20 and 25°, corresponding to the characteristic signatures of ETS-10 [25]. Meanwhile, some distinct peaks of TiO_2 can be observed in the XRD pattern, which indicates excessive anatase was added in the synthesis system. However, the peak intensity of TiO_2 is very small compared with ETS-10, indicating the purity of the ETS-10 is high. The FTIR spectrum of ETS-10 is shown in Fig. 2(b). Among the bands, a wide absorption peak from 2,800 to 3,600 cm^{-1} was observed, which corresponds to symmetrical and anti-symmetrical stretching vibration of -OH in the water molecules. The band near 1,640 cm^{-1} is attributed to the shear motion of water molecules. The absorption peak near 1,039 cm^{-1} represents the asymmetric stretching vibration of the Si-O-Ti chain, while the peak centred at 741 cm^{-1} is ascribed to the telescopic vibration of the Ti-O-Ti chains.

The morphologies of fly ash and prepared ETS-10 are presented in Fig. 2(c) and (d). The SEM image of fly ash shows particles with a wide distribution and spherical morphology. ETS-10 sample, however, displays a truncated bipyramid structure, with a uniform distribution approximately 0.5 (±0.2)×0.2 (±0.2) μm in size. In addition, amorphous phase was hardly noticeable in the SEM image of as-synthesized ETS-10, suggesting the formation of highly crystalline ETS-10. The BET surface area of ETS-10 sample is 246 m^2/g, which is near to the values reported in the literature [26]. The pore size distribution of ETS-10 was measured on a physisorption apparatus (Micromeritics 3 Flex) and represented in Fig. 2(e). From Fig. 2(e), we can conclude that the pore size distribution of as-synthesized ETS-10 sample is concentrated on interval (0-1 nm). Thus, the as-synthesized ETS-10 sample is a kind of microporous material.

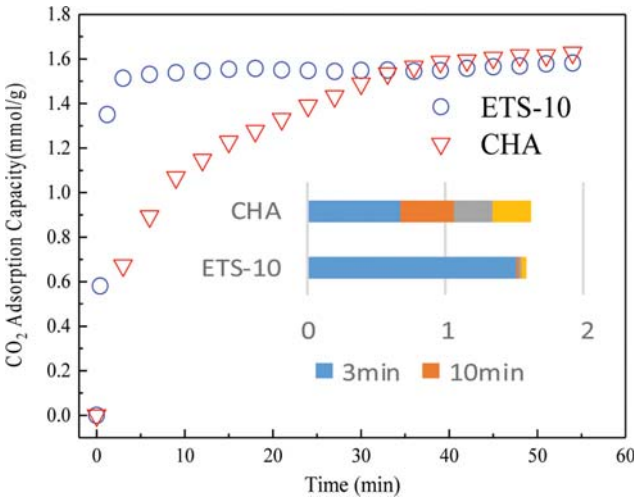

Fig. 3. CO_2 adsorption on the samples at 333 K and 1 bar.

2. CO_2 Adsorption on Fly-ash Based ETS-10

The CO_2 adsorption on prepared ETS-10 at 60 °C was measured by TGA, in comparison with that of zeolite CHA, which was also microporous zeolite derived from fly ash. According to Fig. 3, the equilibrium adsorption capacity of as-synthesized ETS-10 and CHA was 1.59 mmol/g and 1.61 mmol/g, respectively, suggesting that the adsorption loading of CO_2 on the fly-ash based ETS-10 was comparable with other microporous adsorbents. In contrast, the CO_2 uptake of ETS-10 sample reached 1.5 mmol/g in the first 10 min, which consists approximately of 94% of the equilibrium capacity, but the CO_2 uptake of CHA only reached 41% of the equilibrium amount. The adsorption process of ETS-10 was obviously faster, demonstrating remarkable kinetics, which is beneficial to the PSA process.

To investigate the adsorption kinetic process, the obtained experimental data were fitted by different kinetic models, including the pseudo-first order kinetics model and pseudo-second-order kinetics model [27,28]. The kinetic parameters obtained from the fitting results are summarized in Table 1. It is obvious that both kinetic models could describe the CO_2 adsorption process on ETS-10 well, with the correlation coefficient R^2 values greater than 0.99. The equilibrium capacities calculated by both models were all 1.55 $mmol\cdot g^{-1}$, which agreed with the experimental one.

From Fig. 4, the CO_2 adsorption capacity of coal fly ash based ETS-10 is slightly smaller than that of conventional ETS-10. At

Table 1. Parameters of adsorption kinetic simulation results of ETS-10

	q_t=20 min	Pseudo-first order	Pseudo-second order
q_e ($mmol\cdot g^{-1}$)	1.56	1.55	1.55
K ($10^{-2}\cdot min^{-1}$)	-	1.2	5.5
R^2	-	0.9987	0.9979

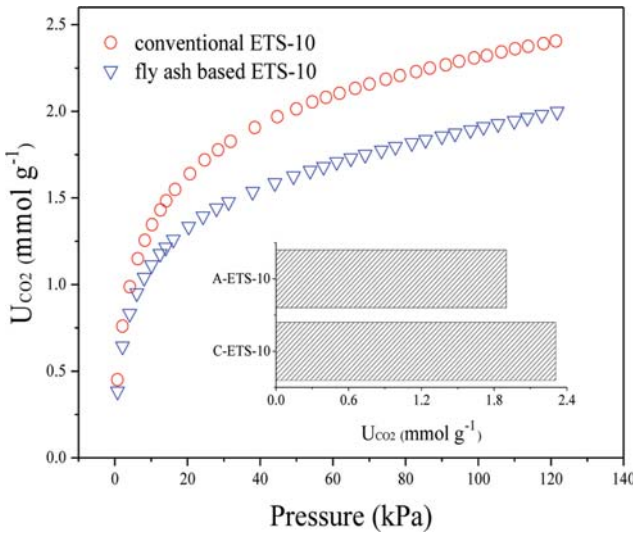

Fig. 4. Single-component adsorption isotherms of CO_2 on coal fly ash based ETS-10 and conventional ETS-10.

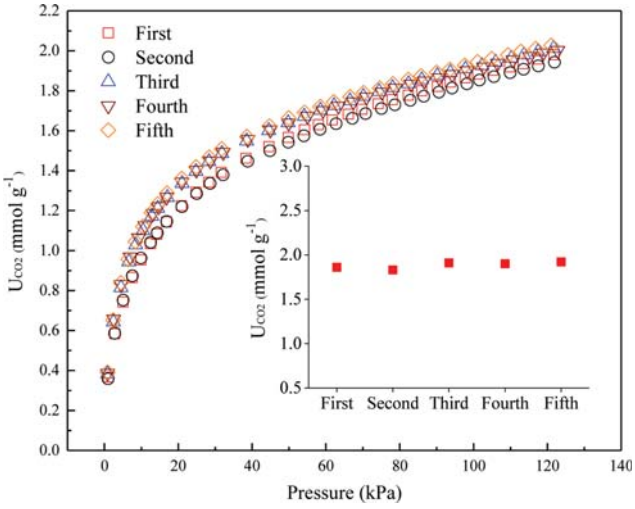

Fig. 6. Adsorption repeatability test of prepared ETS-10.

60 °C and 101 kPa, the CO_2 uptake of fly ash based ETS-10 is 84% of that of conventional ETS-10. Reduction of adsorption properties was inevitable when fly ashes with complicated components were employed, yet the coal fly ash based ETS-10 still retained considerable CO_2 adsorption capacity.

The representative adsorption isotherms for pure component CO_2 over a wide range of temperature (303-393 K) are shown in Fig. 5, and the CO_2 capacity of the sample at 101 kPa is also presented in the inset. At 333 K, the CO_2 capacity was about 1.8 mmol·g^{-1} at 100 kPa. Furthermore, the adsorption capacity of CO_2 decreased with increasing temperature. Raising temperature will exacerbate the thermal movement of CO_2 molecules and the lattices of the adsorbent; thus, a stronger intermolecular force will be required to maintain the adsorption equilibrium. When the interaction between them is not enough to bind CO_2 molecules, a portion of the CO_2 molecules will escape from the pores of the ETS-10. A gradual decrease of CO_2 capacity was observed at this temperature range. However, a relative high uptake of 1.35 mmol·g^{-1} was still obtained at 393 K. This suggests that prepared ETS-10 could be a good adsorbent at high temperature.

Another important feature for the use of ETS-10 for CO_2 adsorption is that ETS-10 can be repeatedly used without obvious performance degradation. To explore the repeatability of ETS-10, five cycles of CO_2 adsorption-desorption were carried out on the physisorption apparatus at 333 K. The representative adsorption isotherms for each time are shown in Fig. 6, and the CO_2 adsorption capacities for each time at 101 kPa are also presented in the inset. From Fig. 6, the coal fly ash based ETS-10 maintained its high CO_2 adsorption capacity after five cycles.

To explore the interaction energy between adsorbent and adsorptive molecules, we used the Clausius-Clapeyron isosteric method to calculate the adsorption heat Q_{st}. The experimental results are

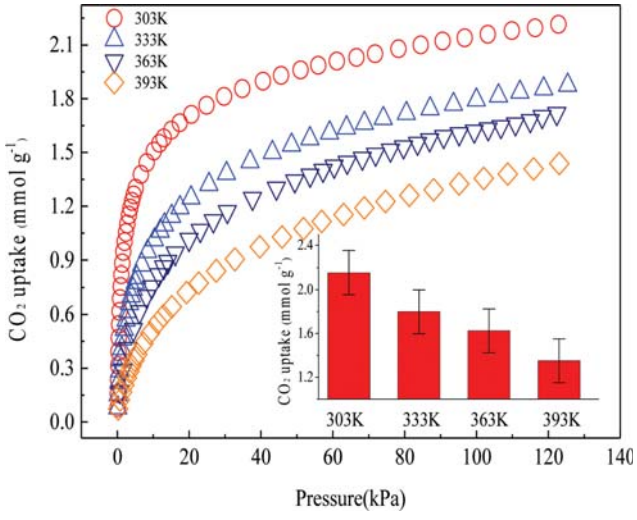

Fig. 5. Single-component adsorption isotherms of CO_2 on prepared ETS-10.

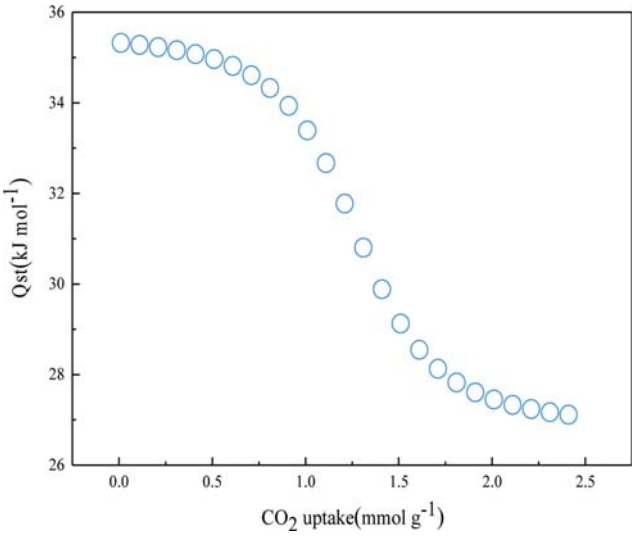

Fig. 7. Uptake-dependent heats of adsorption.

presented as adsorption isotherms and load-dependent heats of adsorption.

In Fig. 7 the uptake-dependent curve of the heat of CO_2 adsorption declines with the uptake. This trend can be attributed to the combination of dispersion interactions and additional quadrupole interactions between the CO_2 double bonds and the ETS-10 cations. The quadrupole-cation interactions are stronger and dominate adsorption at lower uptake. At higher uptake their contribution decreases with increasing distance to the bonding sites on the surface, while the influence of lateral dispersion interactions increases. As a consequence of these additional quadrupole-cation interactions the heat of CO_2 adsorption declines with the CO_2 uptake. From the perspective of heat release, ETS-10 adsorption heat release is high, and that means much energy is required to destroy the connection between CO_2 and ETS-10.

The Gibbs free energy change is a critical factor for determining the degree of spontaneity of a process. If $\Delta G>0$ the total free energy of the system decreases, so the process cannot occur spontaneously at a given temperature. In contrast, if $\Delta G<0$, the process will occur spontaneously at a given temperature [29].

As widely reported [29-31], calculation of Gibbs free energy change in a adsorption process needs to be combined with the experimental data obtained from the Langmuir isotherms. Therefore, the adsorption isotherm was fitted with the Langmuir equation. The mathematical expression of the Langmuir equation is as follows:

$$q=\frac{q_m b P_{CO_2}}{1+bP_{CO_2}} \quad (11)$$

where q_m (mmol g^{-1}) is the maximum-monolayer adsorption capacity of the adsorbent, P_{CO_2} (atm) is the equilibrium pressure of the gas adsorbed, b (atm^{-1}) is the Langmuir adsorption constant.

Gibbs free energy change can be calculated by following equation:

$$\Delta G=-RT\ln K \quad (12)$$

where R is the universal ideal gas constant (8.314 J mol^{-1} K^{-1}), T is the absolute temperature in Kelvin (K), K is the parameter b in Langmuir model fitting.

Table 2. Parameter of Langmuir model fitting and Gibbs free energy change

	b	q_m	R^2	ΔG
	atm^{-1}	mmol·g^{-1}		kJ·mol^{-1}
303 K	43.41	2.05	0.964	−9.504
333 K	13.93	1.83	0.974	−7.296
363 K	6.82	1.822	0.983	−5.797
393 K	4.55	1.603	0.987	−4.952

The calculation results are presented in Table 2. The Gibbs free energy change is negative at given temperatures, indicating that the total free energy of the system decreases and the process can occur spontaneously at the experiment temperatures. Meanwhile, the absolute value of the Gibbs free energy change decreases with the increase of temperature, meaning that the adsorption properties decrease at higher temperatures.

3. Binary Breakthrough Experiments

To assess the impact of moisture on the CO_2 adsorption, CO_2/H_2O binary breakthrough and H_2O single-component breakthrough experiments were conducted at 323 K. The relative humidity (RH) chosen in CO_2/H_2O binary breakthrough experiment was 6% and 25%, respectively. Among them, a relative humidity of 6% could be considered as an optimal industrial application environment, which can be used as a standard of evaluating the performance of ETS-10 sample in industrial environments. In contrast, 25% was chosen to test the adsorption performance of ETS-10 in an extremely bad environment, which can be used as a reference of ability to cope with extreme environments in industrial applications. As shown in Fig. 8, CO_2 breakthrough was an extremely fast process, the CO_2 front moves considerably faster than the water front. The times to breakthrough for CO_2 were 5 s and 20 s, at RH value of 25% and 6%, respectively. As expected, the breakthrough time of CO_2 on the as-synthesized ETS-10 decreased with the increase of RH value. The breakthrough time for water on the ETS-10 sample, however, was extremely slow. The breakthrough time and saturation time of

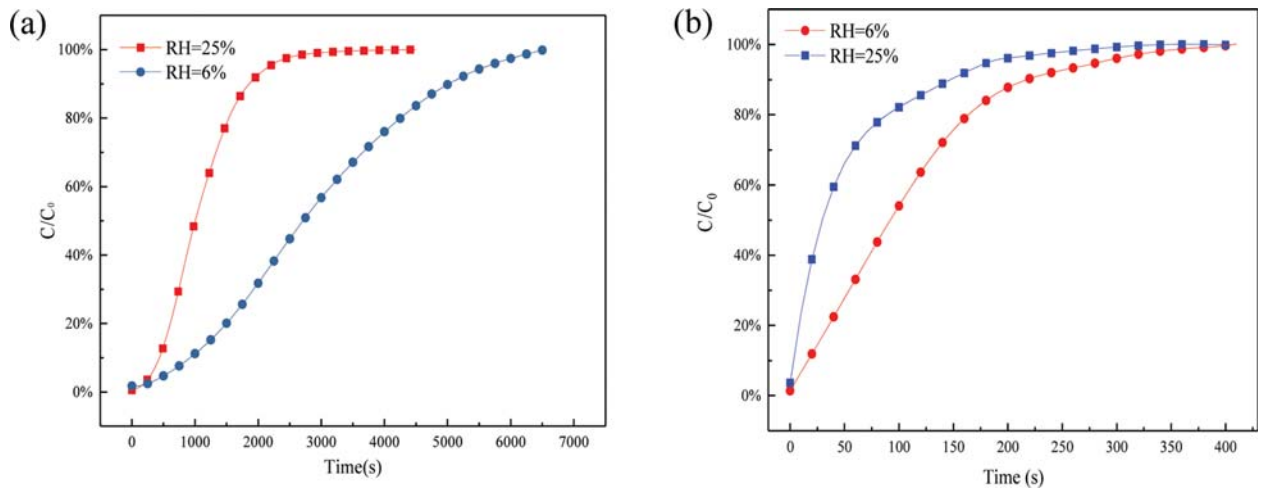

Fig. 8. Binary breakthrough curves of prepared ETS-10 at 323 K (a) H_2O breakthrough curves (b) CO_2 breakthrough curves.

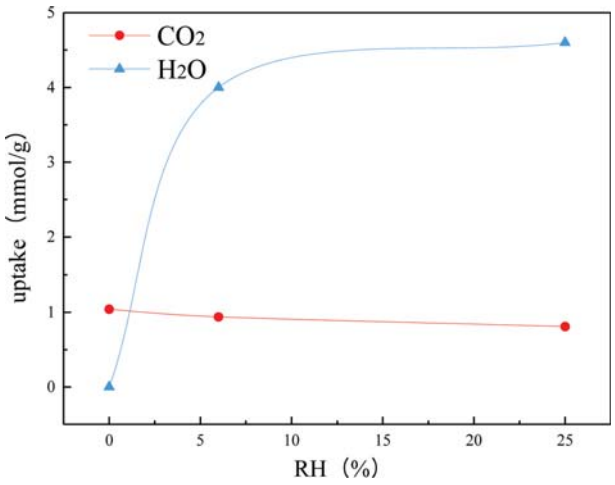

Fig. 9. CO_2/H_2O uptake on prepared ETS-10 at different RH.

water were, respectively, 350 s and 1,645 s at the RH of 25%. This could be attributed to a strong electrode in the channel of ETS-10, and CO_2 has a stronger dipole moment and quadrupole moment, which is easier to occupy the dominant positions in the competitive co-adsorption of water.

Humidity is an important parameter for CO_2/H_2O binary adsorption; therefore, its influences on the CO_2 and H_2O adsorption performance of as-synthesized fly-ash based ETS-10 were carefully investigated. As shown in Fig. 7, in the humidity range of 0, 6 and 25%, the CO_2 capacity on ETS-10 was 1.04, 0.94, and 0.81 mmol·g^{-1}, respectively. As expected, the CO_2 capacity on the prepared sample decreased with increasing humidity. However, the prepared ETS-10 has much higher CO_2 capacity than that of zeolite 13X [32]. For instance, at a lower humidity (6%), the CO_2 adsorption capacity onto ETS-10 was still 0.94 mmol·g^{-1}, indicating that the presence of water vapor has little effect on the CO_2 adsorption capacity of ETS-10. As to its H_2O capacity, we could gain more information from Fig. 9. H_2O uptake increased with the increase of RH value and was lower than other adsorbents. We could conclude that the fly-ash based ETS-10 could be applied in the field as a good adsorbent for capturing CO_2 from humid flue gases.

CONCLUSIONS

High purity ETS-10 was synthesized using coal fly ash as the silicon source. It was confirmed by XRD, FT-IR and SEM, presenting typical ETS-10 crystals, intact Si-O-Si and Ti-O-Ti frameworks and uniform truncated bipyramid structures. The porous product, with a considerable BET surface area of 246 m^2/g, exhibits high CO_2 adsorption capacity and outstanding kinetics. Further CO_2/H_2O binary breakthrough experiments demonstrated that prepared fly-ash based ETS-10 could be a potential adsorbent for capturing CO_2 from humid flue gases due to the consistently favorable adsorption properties at the presence of H_2O.

ACKNOWLEDGEMENTS

The authors gratefully acknowledge the financial support of Natural Science Foundation of China (Grant Nos. 51406029 and 51474067) and also acknowledge Education Department of Liaoning Province (Funding No. LZ2015032) and National Department of Education (Funding No. N172504027) for providing the funding.

REFERENCES

1. H. Sun, Y. Wang, J. Chen, J. Zhai, C. Jing, X. Zeng, H. Ju, N. Zhao, M. Zhan and L. Luo, *Quaternary International*, **453**, 74 (2017).
2. L. Riboldi and O. Bolland, *Energy Procedia*, **114**, 2156 (2017).
3. S. Ga, H. Jang and J. H. Lee, *Comput. Chem. Eng.*, **102**, 188 (2017).
4. M. Clausse, J. Merel and F. Meunier, *Int. J. Greenhouse Gas Control*, **5**(5), 1206 (2011).
5. G. Ferrara, A. Lanzini, P. Leone, M. Ho and D. Wiley, *Energy*, **130**, 113 (2017).
6. D. Zhang, H. Wang, C. Li and H. Meng, *Chem. Eng. Res. Design*, **125**, 361 (2017).
7. Z. Jawad, A. Ahmad, S. Low, R. Lee and P. Tan, *Procedia Eng.*, **148**, 327 (2016).
8. W. L. Queen, E. D. Bloch, J. S. Lee, J. D. Howe, J. A. Mason, M. I. Gonzalez, M. R. Hudson, K. Lee, S. J. Teat and J. B. Neaton, [in] *Proceedings of the Abstracts of Papers, 249th ACS National Meeting Exposition, Denver, CO, United States, March 22-26, 2015*, 2015, PHYS-215.
9. F. Akhtar, S. Ogunwumi and L. Bergström, *Scientific Reports*, **7**(1), 10988 (2017).
10. T.-H. Bae, M. R. Hudson, J. A. Mason, W. L. Queen, J. J. Dutton, K. Sumida, K. J. Micklash, S. S. Kaye, C. M. Brown and J. R. Long, *Energy Environ. Sci.*, **6**(1), 128 (2013).
11. M. M. Lozinska, E. Mangano, J. P. Mowat, A. M. Shepherd, R. F. Howe, S. P. Thompson, J. E. Parker, S. Brandani and P. A. Wright, *J. Am. Chem. Soc.*, **134**(42), 17628 (2012).
12. F. Su and C. Lu, *Energy Environ. Sci.*, **5**(10), 9021 (2012).
13. S. R. Caskey, A. G. Wong-Foy and A. J. Matzger, *J. Am. Chem. Soc.*, **130**(33), 10870 (2008).
14. P. Nugent, Y. Belmabkhout, S. D. Burd, A. J. Cairns, R. Luebke, K. Forrest, T. Pham, S. Ma, B. Space and L. Wojtas, *Nature*, **495**(7439), 80 (2013).
15. O. Shekhah, Y. Belmabkhout, Z. Chen, V. Guillerm, A. Cairns, K. Adil and M. Eddaoudi, *Nature Commun.*, **5**, 4228 (2014).
16. R. Banerjee, A. Phan, B. Wang, C. Knobler, H. Furukawa, M. O'keeffe and O. M. Yaghi, *Science*, **319**(5865), 939 (2008).
17. N. T. Nguyen, H. Furukawa, F. Gándara, H. T. Nguyen, K. E. Cordova and O. M. Yaghi, *Angewandte Chemie*, **126**(40), 10821 (2014).
18. M. Anderson, O. Terasaki, T. Ohsuna, A. Philippou, S. MacKay, A. Ferreira, J. Rocha and S. Lidin, *Nature*, **367**(6461), 347 (1994).
19. S. Uma, S. Rodrigues, I. N. Martyanov and K. J. Klabunde, *Micropor. Mesopor. Mater.*, **67**(2), 181 (2004).
20. J. H. Choi, S. D. Kim, Y. J. Kwon and W. J. Kim, *Micropor. Mesopor. Mater.*, **96**(1), 157 (2006).
21. M. Shi, A. M. Avila, F. Yang, T. M. Kuznicki and S. M. Kuznicki, *Chem. Eng. Sci.*, **66**(12), 2817 (2011).
22. S. J. Datta, C. Khumnoon, Z. H. Lee, W. K. Moon, S. Docao, T. H. Nguyen, I. C. Hwang, D. Moon, P. Oleynikov and O. Terasaki, *Science*, **350**(6258), 302 (2015).
23. E. Glueckauf and J. Coates, *J. Chem. Soc.*, 1315 (1947).

24. Y. Ding and E. Alpay, *Chem. Eng. Sci.*, **55**(17), 3461 (2000).
25. L. Liu, R. Singh, G. Li, P. Xiao, P. Webley and Y. Zhai, *J. Hazard. Mater.*, **195**, 340 (2011).
26. L. Lv, F. Su and X. Zhao, *Micropor. Mesopor. Mater.*, **101**(3), 355 (2007).
27. Q. Zhou, Y. Duan, C. Zhu, J. Zhang, M. She, H. Wei and Y. Hong, *Korean J. Chem. Eng.*, **32**(7), 1405 (2015).
28. H. Haroon, T. Ashfaq, S. M. H. Gardazi, T. A. Sherazi, M. Ali, N. Rashid and M. Bilal, *Korean J. Chem. Eng.*, **33**(10), 2898 (2016).
29. P. Ammendola, F. Raganati and R. Chirone, *Chem. Eng. J.*, **322**, 302 (2017).
30. T. Falayi and F. Ntuli, *Korean J. Chem. Eng.*, **32**(4), 707 (2015).
31. J.-W. Lee, T. P. B. Nguyen and H. Moon, *Korean J. Chem. Eng.*, **23**(5), 812 (2006).
32. G. Li, P. Xiao and P. Webley, *Langmuir*, **25**(18), 10666 (2009).